

This discussion paper is/has been under review for the journal *Atmospheric Chemistry and Physics (ACP)*. Please refer to the corresponding final paper in *ACP* if available.

**Summertime NO_x
measurements
during the CHABLIS
campaign**

S. J.-B. Bauguitte et al.

Summertime NO_x measurements during the CHABLIS campaign: can source and sink estimates unravel observed diurnal cycles?

S. J.-B. Bauguitte^{1,*}, W. J. Bloss^{2,**}, M. J. Evans³, R. A. Salmon¹, P. S. Anderson¹,
A. E. Jones¹, J. D. Lee^{2,***}, A. Saiz-Lopez^{4,****}, H. K. Roscoe¹, E. W. Wolff¹, and
J. M. C. Plane^{4,*****}

¹British Antarctic Survey, Natural Environment Research Council, High Cross,
Madingley Road, Cambridge, CB3 0ET, UK

²School of Chemistry, University of Leeds, Leeds, LS2 9JT, UK

³School of Earth and the Environment, University of Leeds, Leeds, LS2 9JT, UK

⁴School of Environmental Sciences, UEA, Norwich, NR4 7TJ, UK

* now at: Facility for Airborne Atmospheric Measurements, NERC, Cranfield,
Bedfordshire, MK43 0AL, UK

** now at: School of Geography, Earth and Environmental Sciences,
University of Birmingham, Edgbaston, B15 2TT, UK

Title Page

Abstract

Introduction

Conclusions

References

Tables

Figures

⏪

⏩

◀

▶

Back

Close

Full Screen / Esc

Printer-friendly Version

Interactive Discussion

*** now at: Department of Chemistry, University of York, York, YO10 5DD, UK

**** now at: Atomic and Molecular Physics Division, Harvard-Smithsonian
Center for Astrophysics, Cambridge, MA 02138, USA

***** now at: School of Chemistry, University of Leeds, Leeds, LS2 9JT, UK

Received: 17 July 2009 – Accepted: 24 August 2009 – Published: 29 September 2009

Correspondence to: S. J.-B. Bauguitte (s.bauguitte@bas.ac.uk)

Published by Copernicus Publications on behalf of the European Geosciences Union.

ACPD

9, 20371–20406, 2009

**Summertime NO_x
measurements
during the CHABLIS
campaign**

S. J.-B. Bauguitte et al.

Title Page

Abstract

Introduction

Conclusions

References

Tables

Figures

⏪

⏩

◀

▶

Back

Close

Full Screen / Esc

Printer-friendly Version

Interactive Discussion

20372



Abstract

NO_x measurements were conducted at the Halley Research Station, Antarctica, during the austral summer period 1 January–10 February 2005. A clear NO_x diurnal cycle was observed with minimum concentrations close to instrumental detection limit (5 pptv) measured between 04:00–05:00 GMT. NO_x concentrations peaked (24 pptv) between 19:00–20:00 GMT, approximately 5 h after local solar noon. An optimised box model of NO_x concentrations based on production from in-snow nitrate photolysis and chemical loss derives a mean noon emission rate of 3.48×10^8 molecules cm⁻² s⁻¹, assuming a 100 m boundary layer mixing height, and a relatively short NO_x lifetime of ~6.4 h. This emission rate compares to directly measured values ranging from 1.7 to 3.4×10^8 molecules cm⁻² s⁻¹ made on 3 days at the end of the study period. Calculations of the maximum rate of NO₂ loss via a variety of conventional HO_x and halogen oxidation processes show that the lifetime of NO_x is predominantly controlled by halogen processing, namely BrNO₃ and INO₃ gas-phase formation and their subsequent heterogeneous uptake, with a potential smaller contribution from HNO₄ formation and uptake. Furthermore the presence of halogen oxides is shown to significantly perturb NO_x concentrations by decreasing the NO/NO₂ ratio. We conclude that in coastal Antarctica, the potential ozone production efficiency of NO_x emitted from the snowpack is mitigated by the more rapid NO_x loss due to halogen nitrate hydrolysis. These results suggest that the role of halogen oxides need to be considered when interpreting the isotopic signature of nitrate impurities held within snow and ice.

1 Introduction

For the past two decades, polar boundary layer composition and photochemistry has been the focus of major field measurement campaigns undertaken in Arctic and Antarctic research stations.

At Alert (Nunavut, Canada), the pioneering Polar Sunrise Experiments (e.g. Barrie

Summertime NO_x measurements during the CHABLIS campaign

S. J.-B. Bauguitte et al.

Title Page

Abstract

Introduction

Conclusions

References

Tables

Figures

⏪

⏩

◀

▶

Back

Close

Full Screen / Esc

Printer-friendly Version

Interactive Discussion

et al., 1994) initially prompted our attention to boundary layer ozone depletion and Arctic haze pollution events. This triggered further research, such as the Tropospheric Ozone Production around the Spring Equinox (TOPSE) airborne missions flown by the NCAR C-130 research aircraft into the high Canadian Arctic during Spring 2000 (Atlas et al., 2003). Beine and co-workers provided valuable long-term monitoring trends of a variety of pollutants at the NILU-operated Mount Zeppelin station in Svalbard, Eastern Greenland Sea (e.g. Beine et al., 1997). Similar long-term and summer intensive measurements campaign were also conducted at the Summit station on the Greenland icecap (e.g. Dibb et al., 1998, 2002; Honrath et al., 2002).

In Antarctica, Jones et al. (1999) provided the first evidence of snowpack photochemical reactivity when measuring snow-emitted NO_x at the Neumayer coastal station, whereas Davis et al. (2001) provided further observations illustrating the exceptional reactivity of the South Pole boundary layer over the Eastern Antarctic Plateau.

Most of the above-mentioned studies carried out near and over the sea-ice zone have commented on the need to include halogen chemistry in order to reconcile observations and model outputs. The presence of bromine, iodine and chlorine species and their impact on tropospheric ozone is widely acknowledged (von Glasow et al., 2004; Yang et al., 2005; Simpson et al., 2007; Read et al., 2008); our confidence in the ubiquitous impact of halogen chemistry, despite the scarcity of halogens ground-based measurements, has been greatly improved by satellite observations of BrO and IO (Richter et al., 2002; Saiz-Lopez et al., 2007b; Schoenhardt et al., 2008).

It is now accepted that the photolysis of organic and inorganic precursors in the high (and to a lesser extent mid) latitude snowpack contributes to the release and exchange of gas-phase molecules that would hitherto not be expected in the remote polar boundary layer (Dominé and Shepson, 2002; Grannas et al., 2007). This has two main implications: a) the polar boundary layer oxidative capacity is perturbed through ozone and HO_x photochemistry, and b) these post-depositional processes affect the burial rate and chemical signature of deposited ions and trapped trace gases, hence requiring a further degree of constraint for the use of ice core proxies in paleo-atmospheric

**Summertime NO_x
measurements
during the CHABLIS
campaign**S. J.-B. Bauguitte et al.

[Title Page](#)[Abstract](#)[Introduction](#)[Conclusions](#)[References](#)[Tables](#)[Figures](#)[⏪](#)[⏩](#)[◀](#)[▶](#)[Back](#)[Close](#)[Full Screen / Esc](#)[Printer-friendly Version](#)[Interactive Discussion](#)

chemistry modelling studies (Wolff, 1995; Wolff et al., 2008). More recent studies of the stable isotope signature of aerosol (and snow) nitrate have illustrated the complexity in identifying NO_x sources and sinks (Morin et al., 2008 and references therein).

In this study, we describe a set of NO_x measurements conducted at the Clean Air Sector Laboratory (CASLab) at the Halley Research Station, coastal Antarctica, during the CHEMistry of the Antarctic Boundary Layer and Interface with Snow (CHABLIS) campaign (Jones et al., 2008). We focus on the austral summer intensive campaign (1 January–10 February 2005) when comprehensive ancillary HO_x and actinic flux measurements were available. The instrumentation and its performance are first described. We then interpret the mean NO , NO_2 and NO_x diurnal cycles by analysing the contribution of sources and sinks with a simple steady state model. We present results from near snow surface flux measurements of NO_x , and put these in the context of existing measured and model derived fluxes in the Arctic and Antarctic. Our derived NO_x lifetime is compared to sink estimates employing the latest kinetic data of known oxidation processes. We analyse the NO_x partitioning and assess the factors controlling the NO/NO_2 ratio.

2 Methods

2.1 NO_x instrumentation

NO_x measurements were conducted using a 2-channel chemiluminescence (CL) analyser, which evolved from the single channel system described in Cotter et al. (2003). A second CL channel was implemented to allow higher time resolution and simultaneous detection of NO and NO_x .

The design of the NO_2 photolytic converter (PLC) employed in this study was inspired by the narrow-band (ca. 365 nm) photolysis system described in Ryerson et al. (2000), and employs an Oriel PhotoMax lamp housing. The ellipsoid-focussed UV source used during CHABLIS was a more powerful 200 W Hg super high-pressure arc

Summertime NO_x measurements during the CHABLIS campaign

S. J.-B. Bauguitte et al.

Title Page

Abstract

Introduction

Conclusions

References

Tables

Figures

◀

▶

◀

▶

Back

Close

Full Screen / Esc

Printer-friendly Version

Interactive Discussion

**Summertime NO_x
measurements
during the CHABLIS
campaign**S. J.-B. Bauguitte et al.

Title Page

Abstract

Introduction

Conclusions

References

Tables

Figures

⏪

⏩

◀

▶

Back

Close

Full Screen / Esc

Printer-friendly Version

Interactive Discussion

lamp (USHIO 200DP) with water-cooled electrodes, compared with the 75 W Xe-Hg lamp used in previous work (Cotter et al., 2003). This yielded a threefold increase in the NO₂ conversion efficiency. Spectral filtering of the UV output was achieved by means of a Pyrex window (Oriel part number 60127) as a 320 nm UV cut-out, located
5 between the focussed arc and lamp housing. A KBr infrared absorbing filter (KG3, Oriel part number 51960) was also inserted to minimize heat transfer to the photolysis cell. Given the spectral filtering employed in our PLC, we believe that the main photolytic interferent is HONO (Beine et al., 2002 and Ryerson et al., 2000), although we were not able to quantify this potential interference.

10 Cold ambient air was fanned from outside the CASLab and directed onto the NO₂ photolysis quartz cell to maintain its wall temperature below ~12°C. Without this forced air cooling, the cell heated up to temperatures in excess of 50°C. Although we believe that this optical arrangement and the short cell plug-flow residence time (<2 s) minimised the photolysis cell NO₂ artefact from thermal decomposition of labile molecules
15 such as peroxy acetyl nitrate or pernitric acid, we were not able to quantify these potential interferences.

The NO_x measurement duty cycle was optimised as follows. The CL detectors' baseline count rates were determined by pre-chamber zeroing every 10 to 15 min for 60 s. One minute averaged zero count rates were then linearly interpolated, to produce a
20 baseline ready for subtraction from the raw signal count rate. All CL data acquired in 1 Hz photon-counting mode was then reduced to one minute averages after applying baseline, calibration and artefact corrections.

The NO sensitivity of the CL detectors was determined twice daily for 10 min, with a repeat time of 13 h, by standard addition to the ambient air matrix of a 1 ppmv NO/N₂ mixture (UK National Physical Laboratory traceable BOC certified), which is further diluted by mass flow controllers to yield 2 ppbv NO. Using the same calibration schedule,
25 the NO₂ channel photolytic conversion efficiency (CE) was determined by addition of a known mole fraction of NO₂. This was achieved by quantitative gas-phase titration of the NO/N₂ mixture to NO₂ by O₃ generated from a pen-ray Hg lamp, and monitoring

the un-titrated NO mole fraction (typically 5%).

Detector artefact determinations were also performed twice daily with a 13 h repeat time staggered to that of the NO sensitivity calibrations, thereby randomising in time of day the calibration and artefact determination sequences. Instrumental artefacts were determined by overflowing the instrument inlet with scrubbed ambient air supplied by an Eco-Physics Pure Air Generator (model PAG003). Beside a -15°C dew point freeze-drying and ozonation/activated charcoal NO_x filtering stages, this generator type also includes a 350°C heated Palladium catalyst scrubbing stage for the removal of hydrocarbons. We found this method more appropriate than using “ NO_x -free” synthetic compressed air; when comparing our pure air generator output to that of a cylinder of synthetic air (Air Products ZeroPlus grade Air), we found that the measured NO_2 artefact quadrupled (NO artefact doubled) in synthetic air. For all summer data reported here, we subtracted a 2 pptv artefact for NO, and 6 pptv artefact for NO_2 .

The instrumental limit of detection was estimated from the propagation of systematic and random errors. The random error was taken as the one sigma standard error determined when averaging the 1 Hz NO and NO_2 data to one minute means. This standard error therefore corresponds to the measurement precision, and arises largely from Poisson distributed photon-counting statistics, and will decrease with further data averaging.

Overall systematic errors were estimated as the root sum square of all known systematic uncertainties affecting the accuracy of the measurement, namely: $\pm 3\%$ NO calibration gas concentration (mass flow-rate controlled dilution of 1 ppmv NO/N_2 standard gas); error in linear interpolation of the 1 Hz baseline count rate (0.8 and 2.3 pptv for NO and NO_2 , respectively); $\pm 0.4\%$ NO_2 CE determination error; instrumental artefact determination error (± 1 pptv for NO and ± 3 pptv for NO_2).

Table 1 provides a summary of our instrumentation performance parameters and corresponding random and overall systematic errors for NO and NO_2 measurements.

The final NO_x data was filtered for infrequent pollution from the exhaust of the Halley Research Station generators, using the combination of a two-pass wind sector filter

Summertime NO_x measurements during the CHABLIS campaign

S. J.-B. Bauguitte et al.

Title Page

Abstract

Introduction

Conclusions

References

Tables

Figures

⏪

⏩

◀

▶

Back

Close

Full Screen / Esc

Printer-friendly Version

Interactive Discussion

method, station observers' logs, and NO_x data itself. The first pass filter was based on the wind sector exclusion zone (293 to 335°) for all wind speeds, to identify potential "discrete plumes" from the station. The second pass filter was based on the North sector exclusion zone (90 to 270°) for wind speeds <2 m s⁻¹, to identify "dispersed plume". NO_x data was then scanned for possible signs of contamination.

2.2 Flux measurements from snow pack

During three days at the end of the 2004/2005 austral summer (1–4 February 2005), we measured coincident near snow surface NO_x gradients, $\frac{\partial \text{NO}_x}{\partial z}$ (units of pptv m⁻¹) and turbulent diffusivity K (units of m² s⁻¹), which give estimates of vertical NO_x flux, F_{NO_x} , according to:

$$F_{\text{NO}_x} = K \frac{\partial \text{NO}_x}{\partial z} \quad (1)$$

F_{NO_x} is therefore in units of pptv m s⁻¹, a concentration velocity. The NO_x analyser sampled sequentially from two inlets mounted on a mast ~25 m South of the CASLab (see Fig. 1). The upper and lower NO_x inlets were 6.0 m and 1.5 m above the snow surface. Ambient air was drawn back to the CASLab via two ~25 m blacked-out 1/4" od PFA Teflon tubes. The residence time of the ambient air matrix in the PFA transfer lines was measured to be ~14 s, by spiking high NO/N₂ concentrations at the inlet tips. The flow rate through the transfer lines was maintained at ~5 L min⁻¹ with a throttled air pump (GAST model DOA-P725-BN).

For NO_x flux measurements, the instrument duty cycle was modified as follows: 10 min sampling for a particular inlet height, consisting of 9 min measure, and 1 min zeroing, then inlet height swap. The synchronisation of the analyser duty cycle and inlet height switching valves was achieved within 1 to 2 s.

A 30 m turbulence profiling mast was a further 25 m South of the NO_x sampling mast (Fig. 1) with turbulence and mean micro-meteorological sensors mounted in a vertical

Summertime NO_x measurements during the CHABLIS campaign

S. J.-B. Bauguitte et al.

Title Page

Abstract

Introduction

Conclusions

References

Tables

Figures

⏪

⏩

◀

▶

Back

Close

Full Screen / Esc

Printer-friendly Version

Interactive Discussion

array. The instrument set included a sonic anemometer/thermometer at 4 m height above snow. See Anderson and Neff (2008) for a detailed description of the 30 m mast.

Similar sonic anemometry was located 10 m South and 100 m North of the 30 m mast, in order to estimate spatial variability of turbulence measurements at the 4 m level and hence give confidence limits for the diffusivity estimates at the NO_x inlets.

2.3 Photolysis rates

The 2π spectro radiometer used for measuring actinic fluxes is described in Jones et al. (2008). Here we focus on the data processing employed to derive the photolysis rates of atmospheric NO₂ and in-snow nitrate ions, needed for our model study.

2.3.1 JNO₂^{total}

In order to derive the 4π integrated JNO₂^{total}, we used the 2π downwelling JNO₂[↓] (measured routinely), and the 2π upwelling JNO₂[↑] (measured very occasionally). The latter was used to adjust JNO₂[↓] according to the actinic flux ratio (see Jones et al., 2008). For cloudy sky conditions (okta>6.5; cloud cover being estimated as how many eighths of the sky, known by meteorologists as oktas, are obscured by cloud; ranging from completely clear, 0 oktas, through to completely overcast, 8 oktas), we used the actinic flux ratio JNO₂[↓]/JNO₂[↑] equal to 0.98. For less diffuse light conditions (okta<6.5), the ratio was calculated using the solar zenith angle (SZA) parameterisation described in Jones et al. (2008). The correction of the ratio calculated as a function of SZA, to a constant 0.98 actinic flux ratio, was found to be between ±3% and ±14%. The lowest correction figures occurred at low zenith angles and hence high actinic fluxes, while the largest corrections were obtained at high zenith angles. The mean solar noon JNO₂ value for the CHABLIS summer campaign was ~1.93×10⁻² s⁻¹.

Title Page

Abstract

Introduction

Conclusions

References

Tables

Figures

⏪

⏩

◀

▶

Back

Close

Full Screen / Esc

Printer-friendly Version

Interactive Discussion

2.3.2 In-snow $J(\text{Nitrate})^\downarrow$

Estimating and measuring the photolysis rate of nitrate ions in snow is a difficult task (Wolff et al., 2002; Qiu et al., 2002; Fisher et al., 2005). In Wolff et al. (2002) and Jones et al. (2007), NO_x emission rates from snow were estimated using in-snow nitrate ion actinic flux as a function of depth, using a snow pack radiative transfer model (Grenfell, 1991), with the spectral irradiance input, $E^\downarrow(\lambda)$, calculated using the NCAR/ACD radiative transfer model TUV. In their trace gas diffusion modelling study, Anderson and Bauguitte (2007) used global shortwave irradiance measurements, G , for approximating the column integrated in-snow actinic flux for nitrate, defined as $\int J(\text{Nitrate})^\downarrow dz$. They argue the case for the approximate linearity of the transfer function $G \rightarrow \int J(\text{Nitrate})^\downarrow dz$.

The above methodologies suffer from a variety of shortfalls. In the two former studies, inherent uncertainties are introduced by employing the TUV radiative transfer model output $E^\downarrow(\lambda)$ for the flux computation. In the latter study, G is poorly spectrally resolved for the nitrate ion, and the linear relationship of the proxy is dependent upon zenith angle.

In this study, we approximate in-snow nitrate ion actinic fluxes using 2π downwelling, spectrally resolved, atmospheric actinic flux measurements $F(\lambda)^\downarrow$, which we believe provide a more robust proxy. The methodology has nonetheless its own sources of uncertainties which we discuss here.

$J(\text{Nitrate})^\downarrow$ photolysis rates were computed using nitrate ion cross sections, in liquid phase at room temperature, taken from Burley and Johnston (1992), and quantum efficiencies in ice from the formula of Chu and Anastasio (2003), calculated at 5 K intervals from 258 to 278 K.

A further correction of the in-snow photolysis rate is needed, to account for the fact that we only measure downwelling flux $F(\lambda)^\downarrow$, whereas the in-snow flux is the sum of downwelling and upwelling terms. By analogy with the fluxes inside the top of dense cloud (Madronich, 1987), upwelling and downwelling fluxes are everywhere equal in snow, and in the case of diffuse light when one expects equal downwelling fluxes just

Summertime NO_x measurements during the CHABLIS campaign

S. J.-B. Bauguitte et al.

Title Page

Abstract

Introduction

Conclusions

References

Tables

Figures

⏪

⏩

◀

▶

Back

Close

Full Screen / Esc

Printer-friendly Version

Interactive Discussion

below and just above the snow surface, the total in-snow flux is $2 \times F^\downarrow$.

Because the relationship between flux and irradiance for diffuse illumination is given by $F^\downarrow = 2 \times E^\downarrow$, the total in-snow flux is $4 \times E^\downarrow$. In the case of direct light (clear sky and no Rayleigh scattering) Lee-Taylor and Madronich (2002) show that the same relationship holds a few cm down inside the snow pack, irrespective of SZA. Above the snow, $E^\downarrow = F^\downarrow \times \cos(\text{SZA})$, and between 1 January and 10 February 2005, the solar noon SZA varied from 52.6° to 61.4° . The resulting proportionality factor in clear sky conditions and low solar noon SZA will therefore be in the range 0.48 to 0.61, so that the total in-snow flux is 1.91 to $2.44 \times F^\downarrow$.

However we argue that the $F^\downarrow = 2 \times E^\downarrow$ relationship still holds to some extent in more direct light conditions, due to Rayleigh scattering of the atmosphere at a sea-level site, especially in the near-UV part of the spectrum where nitrate ions photolyse (280–320 nm). During the CHABLIS summer intensive campaign, the cloud cover was greater than 6.5 okta for $\sim 60\%$ of the time. Hence we choose total in-snow flux to be $2 \times F^\downarrow$, where F^\downarrow is our $j\text{Nitrate}^\downarrow$ calculated from our measured $F(\lambda)^\downarrow$, and accept a potential for error of perhaps 20% near noon on a few days with fully clear skies.

For the CHABLIS austral summer campaign, we computed a mean solar noon $j\text{Nitrate}^\downarrow$ photolysis rate of $\sim 1.19 \times 10^{-7} \text{ s}^{-1}$, so that our in-snow flux would be $\sim 2.38 \times 10^{-7} \text{ s}^{-1}$. This is approximately a factor 5 smaller than the $\sim 12.5 \times 10^{-7} \text{ s}^{-1}$ values measured by actinometry tubes deployed at Summit Greenland on surface snow on 8 June by Qiu et al. (2002), although the authors do not report absolute measurements uncertainty.

2.4 Ancillary data sets

For model calculations, we employed various data sets for the period 1 January to 10 February 2005 as referred to below. For surface ozone and meteorology parameters, we used the data sets highlighted in Jones et al. (2008). OH and HO₂ data from Bloss et al. (2007) were used for lifetime calculations. Mean diurnally varying IO and BrO

Summertime NO_x measurements during the CHABLIS campaign

S. J.-B. Bauguitte et al.

Title Page

Abstract

Introduction

Conclusions

References

Tables

Figures

⏪

⏩

◀

▶

Back

Close

Full Screen / Esc

Printer-friendly Version

Interactive Discussion

concentrations from DOAS observations (Saiz-Lopez et al., 2007a) were used for the extended Leighton relationship calculations. The mean noon-time IO and BrO mixing ratios were respectively 4.3 and 3.8 pptv, with non-zero mixing ratios for $SZA > 90^\circ$ respectively 0.5 and 1.4 pptv (A. Saiz-Lopez and A. Mahajan, personal communication, 2006).

Unless otherwise stated in the text, all kinetic data used for model calculations in this study were taken from JPL Evaluation Number 15 (Sanders et al., 2006).

3 NO_x observations

3.1 Timeseries

The hourly mean NO and NO₂ mixing ratios (pptv) between 1 January and 10 February 2005, calculated from one minute pollution-filtered data, are plotted in Fig. 2.

NO mixing ratios, plotted in red, rarely go above 20 pptv and display a diurnal cycle, anti-correlating with SZA, plotted in grey. This concentration range (0 to 40 pptv) is in contrast to the high concentrations (up to 500 pptv) reported at South Pole over continental Antarctica (Davis et al., 2001, 2004), but in agreement with other coastal Antarctic NO observations (up to 15 pptv) made at the Neumayer Station (Jones et al., 2000; Weller et al., 2002).

NO₂ mixing ratios, plotted in blue against the right-hand axis with a positive offset for clarity, also show a diurnal cycle, although it is not as distinct as that of NO. At times, particularly at the beginning and end of the 40 day measurement period, NO₂ hourly means appear negative. This is due to the incorporation in our analysis of all NO₂ data, regardless of values below detection limit resulting from poor artefact correction, and hence increased systematic uncertainty when atmospheric NO₂ approaches the detection limit of the instrument (~4 pptv, see Table 1).

Summertime NO_x measurements during the CHABLIS campaign

S. J.-B. Bauguitte et al.

Title Page

Abstract

Introduction

Conclusions

References

Tables

Figures

◀

▶

◀

▶

Back

Close

Full Screen / Esc

Printer-friendly Version

Interactive Discussion

3.2 Mean diurnal cycle

Using the observations of Fig. 2, the hourly mean diurnal cycles of NO, NO₂ and NO_x, averaged over the whole dataset, were derived and plotted in Fig. 3. Two-sigma standard errors of the mean ($2\sigma/\sqrt{n}$) were computed for each hourly bin and plotted as the error bars. Both NO and NO₂, and hence NO_x, exhibit clear diurnal cycles, a phenomenon which has been widely reported in previous polar studies (Jones et al., 1999; Jacobi et al., 2000; Ridley et al., 2000; Beine et al., 2002; Weller et al., 2002). In our study, the NO_x mean diurnal cycle is very pronounced. Maximum concentrations of ~24 pptv are observed between 19:00 and 20:00 GMT, and minimum concentrations close to instrumental detection limit are observed in the early hours between 05:00 and 06:00 GMT. It is worth noting that maximum NO_x values occur ~5 h after the local solar noon at 13:45 GMT.

4 Steady state NO_x calculations

4.1 Model description

To understand the factors driving the shape and timing of the observed NO_x diurnal cycle, we consider a simple model based on our current understanding of the photochemistry of polar tropospheric NO_x (Honrath et al., 1999; Cotter et al., 2003; Jones et al., 2007). NO_x is emitted from the snow pack at a rate proportional to the photolysis of nitrate ions in the snow $F(\text{Nitrate})$, equal to $2\times$ our measured $j\text{Nitrate}^\downarrow$ (see Sect. 2.3), with proportionality constant α . We balance this term with a constant loss rate defined by a daily mean NO_x lifetime τ which represents all unspecified losses of NO_x. Our simple model parameterisation is expressed in Eq. (2) below:

$$\frac{\partial [\text{NO}_x]}{\partial t} = \left(\alpha E (\text{Nitrate})^\downarrow \right) - \left(\frac{[\text{NO}_x]}{\tau} \right) \quad (2)$$

Title Page

Abstract

Introduction

Conclusions

References

Tables

Figures

⏪

⏩

◀

▶

Back

Close

Full Screen / Esc

Printer-friendly Version

Interactive Discussion

The production term scaling factor α has the same dimension as $[\text{NO}_x]$, while $E(\text{Nitrate})^\dagger$ is in s^{-1} .

To model NO_x concentrations, we can integrate Eq. (2) forwards until a diurnal steady state is reached in typically 2 days. We optimize the value of α and τ by minimising a cost function between the hourly model values and the hourly observed values to provide the best possible fit to the diurnal hourly observations in Fig. 3, as described in Eq. (3):

$$\text{Cost} = \sum_{\text{hours } 0-24} |[\text{Model}] - [\text{Obs}]| \quad (3)$$

This minimisation is achieved using the Powell method described in Sect. 10.5 of Press et al. (1993). Figure 3 shows the comparison between the observed diurnal variation of NO_x (solid black line) and the best fit values of the model (dashed black line). After optimization the model simulation reproduces many of the features observed, including the early morning NO_x minimum, and the NO_x peak after solar noon.

4.2 Results: NO_x production term

Using the method described above, we compute a value of 5516 pptv for α , and a value of 6.38 h for τ . Assuming a 100 m boundary layer mixing height (annual mean height for Halley is ~ 70 m, Jones et al., 2008), α corresponds to a mean noon emission rate of 3.48×10^8 molecules $\text{cm}^{-2} \text{s}^{-1}$ for the 1 January to 10 February 2005.

Snow pack NO_x flux measurements from previous polar studies are summarised in Table 2. Our model noon NO_x emission rate is in good agreement with fluxes measured for instance by Jones et al. (2001), who report noon-time NO_x flux maxima of 3×10^8 molec $\text{cm}^{-2} \text{s}^{-1}$ at Neumayer.

Using a snow pack radiative transfer model methodology, Jones et al. (2007) estimated a daily average emission rate of 1.92×10^8 molec $\text{cm}^{-2} \text{s}^{-1}$ for 18 January 2005 during CHABLIS.

Summertime NO_x measurements during the CHABLIS campaign

S. J.-B. Bauguitte et al.

Title Page

Abstract

Introduction

Conclusions

References

Tables

Figures

⏪

⏩

◀

▶

Back

Close

Full Screen / Esc

Printer-friendly Version

Interactive Discussion

Evans et al. (2003) modelled the High Canadian Arctic (>55° N) observations made during the TOPSE airborne campaign in March–May 2000. Their daily averaged model-derived NO_x flux was equivalent to 3.6×10⁸ cm² s⁻¹ for a 200 m boundary layer height.

We conducted NO_x flux measurements for several days at the end of the CHABLIS summer campaign (see Methods). The 20 min averaged NO_x gradients, defined as $\frac{\partial \text{NO}_x}{\partial z}$, where $\partial z=4.5$ m (NO_x sampling inlets height differential) are presented in panel a of Fig. 4. Coincident averaged surface diffusivity K (m² s⁻¹) is plotted in panel b. K was defined as the product $k \times z \times U_*$, where $k=0.4$ is the dimensionless von Karman constant, U_* is the friction velocity (m s⁻¹) defined as the cross product of sonic anemometer data, and $z=4$ m is the height of the turbulence sensor (see Fig. 1). The NO_x flux is defined by the product of the gradient and surface diffusivity (Anderson and Neff, 2008). 20 min averaged NO_x fluxes (in molec cm⁻² s⁻¹) are plotted in panel c of Fig. 4. The daily mean NO_x fluxes measured during the period 1–4 February 2005 ranged from 1.7 to 3.4×10⁸ molec cm⁻² s⁻¹ (see Table 2), again in good agreement with the flux derived from our steady state NO_x analysis.

5 NO_x lifetime calculations

5.1 Model description

Our estimated NO_x emission flux is consistent with previous studies. However our estimated daily mean NO_x lifetime of 6.38 h appears relatively short given known NO_x losses. Using available observations, we consider the maximum rate of NO₂ loss via a variety of conventional HO_x and halogen oxidation processes:



20385

Summertime NO_x measurements during the CHABLIS campaign

S. J.-B. Bauguitte et al.

Title Page

Abstract

Introduction

Conclusions

References

Tables

Figures

⏪

⏩

◀

▶

Back

Close

Full Screen / Esc

Printer-friendly Version

Interactive Discussion





All of these sinks represent NO_2 losses. To convert the NO_2 losses to a NO_x lifetime we use Eq. (4) (Seinfeld and Pandis, 1998):

$$\tau_{\text{NO}_x} = (k_i [\text{Oxidant}])^{-1} \left(1 + \frac{[\text{NO}]}{[\text{NO}_2]} \right) \quad (4)$$

where k_i is the oxidation rate constant for reaction R_i . HO_x observations reported in Bloss et al. (2007) were used for Reactions (1) and (3). For Reactions (4) and (5), we assumed a constant 3 pptv IO and 3 pptv BrO sensitivity level, consistent with the DOAS summertime observations conducted by Saiz-Lopez et al. (2007a).

5.2 Results

Equation (4) now allows us to calculate the NO_x lifetimes for each reaction and how they vary around the day. This is shown in Fig. 5. The conventional NO_x loss pathways, HNO_3 and NO_3 formation represented by the red and blue lines, are much too slow to be significant. They suggest NO_x lifetimes of the order of at least 100 h whereas the observations suggest a lifetime of ~ 6 h. HNO_4 formation (green line) offers a potentially more efficient loss process. Once sequestered in the HNO_4 reservoir, further aerosol uptake and hydrolysis is required to ultimately remove NO_x . However, even assuming that photolysis and thermal decomposition of HNO_4 is negligible compared to aerosol uptake, the mean NO_x lifetime would be of the order of 20 h, still significantly longer than that derived from the observations.

Given the observed concentrations of IO and BrO during CHABLIS, the production of halogen nitrates appears to be the most significant sink for NO_x , as indicated by the black and grey lines in Fig. 5. The NO_x lifetime to these reactions is very short,

Title Page

Abstract

Introduction

Conclusions

References

Tables

Figures

⏪

⏩

◀

▶

Back

Close

Full Screen / Esc

Printer-friendly Version

Interactive Discussion



with a combined diurnal mean lifetime approaching half an hour, fast enough to explain the steady state derived diurnal mean lifetime of ~ 6 h. However, for the production of halogen nitrates to act as a net NO_x sink, the halogen nitrates must hydrolyse on the surface of aerosol. This process competes with their photolysis. These two processes are now considered.

5.3 Heterogeneous loss lifetime calculations

We estimate the lifetime of halogen nitrates and pernitric acid to their heterogeneous uptake in the aerosol phase. This treatment is similar to that used in the 1-D box modelling study of Saiz-Lopez et al. (2008) and zero-D box modelling study of Bloss et al. (2009), whereby the uptake to aerosol represents irreversible loss from the gas phase, and subsequent condensed-phase (hydrolysis) reactions are not specified. We use the free molecular transfer theory and estimate the heterogeneous uptake rate constant k_{het} using Eq. (5):

$$k_{\text{het}} = \frac{\bar{c}\gamma SA}{4} \quad (5)$$

where \bar{c} is the mean gas velocity, γ is the reaction probability, and SA is the aerosol surface area.

Physical properties of aerosol particles were not measured during CHABLIS. However aerosol surface area measurements were reported by Davison et al. (1996) on board the Royal Research Ship Bransfield moored along the Brunt Ice Shelf near Halley, between 21 and 31 December 1992. The mean geometric aerosol surface area for measurements made south of 58° S with an ASASP-X volatility analyser was $\sim 0.32 \pm 0.01 \times 10^{-7} \text{ cm}^2 \text{ cm}^{-3}$. The authors argue that the ASASP-X technique only measures the “dry” geometric aerosol SA for the accumulation mode size range 0.1 to $0.4 \mu\text{m}$ diameter, and therefore does not represent the full aerosol size range (0.1 to $3 \mu\text{m}$). The actual SA is likely to be higher and varying with relative humidity, up to 4 times for 75–80% RH. The studies of Saiz-Lopez et al. (2008) and Bloss et al. (2009)

Summertime NO_x measurements during the CHABLIS campaign

S. J.-B. Bauguitte et al.

Title Page

Abstract

Introduction

Conclusions

References

Tables

Figures

⏪

⏩

◀

▶

Back

Close

Full Screen / Esc

Printer-friendly Version

Interactive Discussion



used an SA of $10^{-7} \text{ cm}^2 \text{ cm}^{-3}$, and we used the same value, in line with the above findings.

We assume the same dimensionless γ reaction probability for both BrNO_3 and INO_3 of 0.8 (Sander et al., 2006), and 0.1 for HNO_4 (Li et al., 1996). Using Eq. (5), we compute daily mean lifetimes to heterogeneous uptake of 4.1, 0.7 and 0.8 h for HNO_4 , BrNO_3 and INO_3 , respectively. Given the lifetimes derived from the gas-phase formation of HNO_4 or XNO_3 (green, black and grey lines in Fig. 5), the rate limiting step for NO_x loss is the gas-phase formation. These lifetimes now need to be compared to the loss due to photolysis.

5.4 Photolysis effects

Using the radiative transfer model described in Saiz-Lopez et al. (2008), we estimate a maximum noon-time $J\text{HNO}_4$ value of $5.05 \times 10^{-6} \text{ s}^{-1}$, corresponding to a photolysis lifetime greater than 2 days, which is therefore negligible. We use the parameterisation of Bloss et al. (2009) for estimating the photolysis rates of halogen species, based on the TUV radiative transfer model and our $J\text{NO}_2^{\text{total}}$ measurements. At solar noon, we find that INO_3 and BrNO_3 photolyse rapidly (lifetimes $\sim 2\text{--}5$ min), whereas during low insolation hours the BrNO_3 and INO_3 photolysis lifetimes increase to ~ 1 h and ~ 20 min respectively, thus approaching the time scales for XNO_3 hydrolysis. Although the photolysis of the halogen nitrates dominates over their heterogeneous loss during high insolation hours, at greater solar zenith angles the two processes are able to compete efficiently, allowing the heterogeneous uptake of halogen nitrates to occur rapidly, precisely at the time when one expects NO_x net loss pathways to dominate, as indicated by the sharp drop in NO_x mixing ratios in the mean diurnal cycle in Fig. 3.

Summertime NO_x measurements during the CHABLIS campaign

S. J.-B. Bauguitte et al.

Title Page

Abstract

Introduction

Conclusions

References

Tables

Figures

⏪

⏩

◀

▶

Back

Close

Full Screen / Esc

Printer-friendly Version

Interactive Discussion

6 NO/NO₂ ratios

6.1 Observed NO to NO₂ ratios

We now turn our attention from the evolution of the NO_x concentration to that of the NO to NO₂ partitioning. We derive observed hourly NO/NO₂ ratios from 1 min data, as shown by the solid black line in Fig. 6. The highest ratios (2.2±0.2, 2σ standard error) are measured between 10:00 and 11:00, whereas the lowest ratios (0.32±0.04) occur between 02:00 and 03:00. We expect our observed NO/NO₂ diurnal cycle to be centred around solar noon (i.e. maximum JNO_2). However the inclusion of all NO₂ data (i.e. also close to/below detection limit), is affecting the shape of our diurnal cycle (see Sect. 3). Here we focus chiefly on the magnitude of the ratios.

6.2 “Classic” Leighton relationship

Classically the NO to NO₂ ratio is defined solely by the steady state reaction between NO and O₃, and NO₂ photolysis; this relationship is known as the Leighton relationship (Leighton, 1961). The reaction rates of NO+HO₂ and NO+RO₂ are negligible compared to the reaction with O₃ (<2% contribution to NO→NO₂ cycling). Hence:

$$\frac{[NO]}{[NO_2]} = \frac{JNO_2^{\text{total}}}{k_{O_3} [O_3]} \quad (6)$$

The NO/NO₂ ratios calculated by this method are shown in Fig. 6 as the solid red line. This reveals a large discrepancy between observed and calculated NO/NO₂, with calculated ratios being almost three times higher at local noon.

6.3 “Extended” Leighton relationship – halogen effects

The reaction between halogen oxide radicals (XO) and NO is rapid and has been shown in previous studies to impact NO/NO₂ ratios (e.g. Ridley et al., 2000; Evans

Title Page

Abstract

Introduction

Conclusions

References

Tables

Figures

⏪

⏩

◀

▶

Back

Close

Full Screen / Esc

Printer-friendly Version

Interactive Discussion



et al., 2003; Ridley and Orlando, 2003; Saiz-Lopez et al., 2008). The discrepancy between observed and the “classic” Leighton relationship ratios reflects the halogen oxides reacting with NO to create NO₂. Equation (6) can be altered to reflect this extra chemistry given by the “extended” Leighton relationship:

$$\frac{[\text{NO}]}{[\text{NO}_2]} = \frac{J\text{NO}_2^{\text{total}}}{k_{\text{O}_3} [\text{O}_3] + k_{\text{BrO}} [\text{BrO}] + k_{\text{IO}} [\text{IO}]} \quad (7)$$

Using diurnally varying BrO and IO (see Methods) and Eq. (7), we calculate NO/NO₂ ratios as shown in Fig. 6 by the dotted red line. The inclusion of halogen oxides in our calculations markedly decreases the ratio and brings it into agreement with our observations. Thus halogen oxides play a highly significant role in decreasing the NO/NO₂ ratio.

Noon-time NO/NO₂ ratios measured at Neumayer in February 1999 (Jones et al., 2000) were even lower (~0.75) than our observed ratios, suggesting that the impact of XO chemistry in controlling NO_x partitioning at Neumayer might be even more pronounced than at Halley.

At Alert in the high Canadian Arctic, Ridley et al. (2000) observed diurnally varying NO/NO₂ in March–April 1998, with ratios reaching up to ~0.5 at low SZA (75°). The authors calculated a ≤10 pptv burden for radicals (HO₂+RO₂+BrO+ClO) in order to sustain their observed low ratios. It is worth remembering that these observations were carried out in Springtime, at a time when BrO is expected to be at its peak.

Our results also corroborate those of the Saiz-Lopez et al. (2008) halogen chemical and transport modelling study, in which their model was constrained with a NO_x summertime flux of 2 × 10⁸ molecules cm⁻² s⁻¹, assumed to be produced by photochemistry of snow pack nitrate. Without halogen chemistry, they estimate a solar noon NO/NO₂ ratio of ~3.3, which then drops to ~1.8 after implementation of the halogen chemistry scheme.

Summertime NO_x measurements during the CHABLIS campaign

S. J.-B. Bauguitte et al.

Title Page

Abstract

Introduction

Conclusions

References

Tables

Figures

⏪

⏩

◀

▶

Back

Close

Full Screen / Esc

Printer-friendly Version

Interactive Discussion

7 Discussion

We showed that our observed mean NO_x diurnal cycle can be reproduced using a simple chemical steady state NO_x analysis, with realistically quantified NO_x emission rates from snow, and identified viable NO_x chemical loss pathways leading to short NO_x lifetimes. A different approach was used by Anderson and Bauguitte (2007) who employed a simple boundary layer tracer diffusion model to investigate how the NO_x diurnal cycle, observed during distinct cloud free and cloud cover periods, could be explained by simple meteorological parameterisation. They show that the shape of the diurnal cycle, in particular the phase offset (from local noon) of the concentration maximum, can be reproduced by tuning a τ value, defined as the rate of (unspecified) tracer decay in a gradient-free environment, and also by assessing the potential effect of a variable boundary layer depth.

Both our methodology in the present paper and that of Anderson and Bauguitte (2007) use simplified models with inherent caveats. While assuming a fixed 100 m boundary layer depth for deriving our model NO_x flux (see Sect. 4.2), with “near-instant” vertical mixing, we clearly ignore the atmospheric boundary layer physics highlighted in the Anderson and Bauguitte (2007) study. Conversely, the latter physics-based study acknowledges under-representing the highly complex underlying NO_x – HO_x and halogen chemistry. It is most probable that a truer representation of our observations requires a combined approach from the chemistry and physics point-of-view.

Our NO_x lifetime study identified apparent NO_2 oxidation loss pathways involving pernitric acid and halogen nitrates, and their aerosol uptake. Although the parameterisation of these processes entails uncertainties (aerosol surface area, reaction probability), we show that the kinetics are sufficiently fast to explain the relatively short NO_x lifetimes initially derived from our steady state calculations. Evans et al. (2003) modelled the Arctic observations made during the TOPSE airborne campaign, and identified HNO_4 formation, aerosol uptake and hydrolysis as the dominant NO_x loss process in the Arctic boundary layer in spring. Under halogen-free conditions, this study finds

Summertime NO_x measurements during the CHABLIS campaign

S. J.-B. Bauguitte et al.

Title Page

Abstract

Introduction

Conclusions

References

Tables

Figures



Back

Close

Full Screen / Esc

Printer-friendly Version

Interactive Discussion

that the HNO_4 loss channel can account for up to 50% of the NO_x loss at noon. They also inferred some contribution from BrNO_3 formation and uptake/hydrolysis.

It is noteworthy that the NO_x diurnal cycle does not appear to be affected by extreme changes in the local atmosphere and snow surface, such as during the 7–10 January 2005 period, when the blizzard wind speeds in excess of 15 m s^{-1} and blowing snow were experienced (see Fig. 2). Even under such extreme conditions, neither the amplitude nor the timing of the diurnal maximum are outside the range of more quiescent conditions. In these very turbulent atmospheric conditions, we expect well-diffused light photolysis of wind-blown snow particles, and therefore NO_x production would be occurring. Snow pack wind pumping would presumably maintain an efficient NO_x diffusion and mixing in the overlying boundary layer. Equally the process of NO_x loss by heterogeneous uptake to the aerosol phase of pernitric acid and halide nitrates would still be ongoing with enhanced aerosol scavenging.

The impact of the source of NO_x from snow photolysis on the Antarctic boundary layer composition might be expected to lead to O_3 production; however in coastal regions the halogens tend to mitigate this effect due to the reduced NO_x lifetime and a reduction in the NO/NO_2 ratio. Away from marine influences, the impact of photolysis of snow phase nitrate is significantly different as can be seen at the South Pole (Crawford et al., 2001; Jones and Wolff, 2003). The geographical extent to which halogens mitigate the impact is as yet unknown.

The impact of halogens on HO_x and O_x chemistry in coastal Antarctica, the Arctic and mid-latitudes is well documented (e.g. Sjostedt et al., 2007; Grannas et al., 2007; Simpson et al., 2007; Saiz-Lopez et al., 2008; Read et al., 2008). However, the impact on NO_x is less well characterised. It seems clear from this study that, in coastal Antarctica, the impact on NO_x lifetime and partitioning is also significant. This result may signal an influence that is active beyond the Antarctic coastal region and into the global marine boundary layer on climate-relevant parameters such as O_3 and OH .

Summertime NO_x measurements during the CHABLIS campaign

S. J.-B. Bauguitte et al.

[Title Page](#)[Abstract](#)[Introduction](#)[Conclusions](#)[References](#)[Tables](#)[Figures](#)[Back](#)[Close](#)[Full Screen / Esc](#)[Printer-friendly Version](#)[Interactive Discussion](#)

8 Conclusions

At Halley, the source of NO_x is mainly a local photochemically driven emission from the snow pack. However observed concentrations peak relatively close to solar noon (~ 5 h) suggesting a much shorter lifetime than is possible through simple HO_x - NO_x photochemistry alone. The shorter lifetime (~ 6 h) is consistent with halogen photochemistry, notably conversion into halogen nitrate, with some contribution from HNO_4 . Given the lack of an observational constraint, the fate of these halogen nitrates is uncertain though heterogeneous uptake onto aerosol and subsequent deposition seems a viable mechanism in this region to return nitrate to the snow surface. This is a dominant uncertainty in evaluating the NO_x budget.

The halogen chemistry also significantly perturbs the NO to NO_2 ratio resulting in much lower NO concentrations than would be otherwise observed, for instance in inland Antarctica. The presence of halogens in the coastal Antarctic region therefore mitigates the atmospheric response of the photochemical NO_x emissions from snow.

A significant implication of these findings is that halogen oxidation influencing the cycling of NO to NO_2 , and ultimately NO_2 loss, will affect the isotopic signature of archived nitrate impurities held within snow and ice.

Acknowledgements. We wish to thank the Halley 2004/05 overwintering staff, in particular Craig Nicholls and Vanessa O'Brien for being so understanding and patient in the overcrowded Clean Air Sector Laboratory. We also thank Steve Colwell for providing meteorological data. This work was funded by the UK Natural Environment Research Council Antarctic Funding Initiative (grant number $\text{NER/G/S/2001/00010}$) and by the British Antarctic Survey core-funded projects SAGES-AIR and CACHE-CEFAC.

References

Anderson, P. S. and Bauguitte, S. J.-B.: Behaviour of tracer diffusion in simple atmospheric boundary layer models, *Atmos. Chem. Phys.*, 7, 5147–5158, 2007, <http://www.atmos-chem-phys.net/7/5147/2007/>.

20393

ACPD

9, 20371–20406, 2009

Summertime NO_x measurements during the CHABLIS campaign

S. J.-B. Bauguitte et al.

Title Page

Abstract

Introduction

Conclusions

References

Tables

Figures

⏪

⏩

◀

▶

Back

Close

Full Screen / Esc

Printer-friendly Version

Interactive Discussion



- Anderson, P. S. and Neff, W. D.: Boundary layer physics over snow and ice, *Atmos. Chem. Phys.*, 8, 3563–3582, 2008, <http://www.atmos-chem-phys.net/8/3563/2008/>.
- Barrie, L. A., Bottenheim, J. W., and Hart, W. R.: Polar Sunrise Experiment 1992 (PSE-1992) – Preface, *J. Geophys. Res.*, 99(D12), 25313–25314, 1994.
- 5 Beine, H. J., Jaffe, D. A., Herring, J. A., Kelley, J. A., Krognes, T., and Stordal, F.: High-latitude springtime photochemistry. Part I: NO_x, PAN and ozone relationships, *J. Atmos. Chem.*, 27, 127–153, 1997.
- Beine, H. J., Honrath, R. E., Dominé, F., Simpson, W. R., and Fuentes, J. D.: NO_x during background and ozone depletion periods at Alert: Fluxes above the snow surface, *J. Geophys. Res.*, 107(D21), 4584, doi:10.1029/2002JD002082, 2002.
- 10 Bloss, W. J., Lee, J. D., Heard, D. E., Salmon, R. A., Bauguitte, S. J.-B., Roscoe, H. K., and Jones, A. E.: Observations of OH and HO₂ radicals in coastal Antarctica, *Atmos. Chem. Phys.*, 7, 4171–4185, 2007, <http://www.atmos-chem-phys.net/7/4171/2007/>.
- Bloss, W. J., Camredon, M., Lee, J. D., Heard, D. E., Saiz-Lopez, A., Plane, J. M. C., Bauguitte, S. J.-B., Salmon, R. A., and Jones, A. E.: A Modelling Study of Radical Chemistry in the Antarctic Boundary Layer, *J. Geophys. Res.*, in preparation, 2009.
- 15 Burley, J. D. and Johnston, H. S.: Ionic mechanisms for heterogeneous stratospheric reactions and ultraviolet photoabsorption cross-sections for NO₂⁺, HNO₃, and NO₃⁻ in sulfuric-acid, *Geophys. Res. Lett.*, 19(13), 1359–1362, 1992.
- 20 Chu, L. and Anastasio, C.: Quantum yields of hydroxyl radical and nitrogen dioxide from the photolysis of nitrate on ice, *J. Phys. Chem. A*, 107(45), 9594–9602, 2003.
- Cotter, E. S. N., Jones, A. E., Wolff, E. W., and Bauguitte, S. J.-B.: What controls photochemical NO and NO₂ production from Antarctic snow? Laboratory investigation assessing the wavelength and temperature dependence, *J. Geophys. Res.*, 108(D4), 4147, doi:10.1029/2002JD002602, 2003.
- 25 Crawford, J. H., Davis, D. D., Chen, G., Buhr, M., Oltmans, S., Weller, R., Mauldin, L., Eisele, F., Shetter, R., Lefer, B., Arimoto, R., and Hogan, A.: Evidence for photochemical production of ozone at the South Pole surface, *Geophys. Res. Lett.*, 28(19), 3641–3644, 2001.
- Davis, D., Chen, G., Buhr, M., Arimoto, R., Hogan, A., Eisele, F., Mauldin, L., Tanner, D., Shetter, R., Lefer, B., and McMurry, P.: Unexpected High Levels of NO Observed at South Pole, *Geophys. Res. Lett.*, 28(19), 3625–3628, 2001.
- 30 Davis, D., Nowak, J. B., Chen, G., Buhr, M., Crawford, J., Lenschow, D., Lefer, B., Shetter, R., Eisele, F., Mauldin, L., and Hogan, A.: South Pole NO_x Chemistry: An assessment of factors

**Summertime NO_x
measurements
during the CHABLIS
campaign**S. J.-B. Bauguitte et al.

[Title Page](#)[Abstract](#)[Introduction](#)[Conclusions](#)[References](#)[Tables](#)[Figures](#)[⏪](#)[⏩](#)[◀](#)[▶](#)[Back](#)[Close](#)[Full Screen / Esc](#)[Printer-friendly Version](#)[Interactive Discussion](#)

**Summertime NO_x
measurements
during the CHABLIS
campaign**

S. J.-B. Bauguitte et al.

Title Page

Abstract

Introduction

Conclusions

References

Tables

Figures

◀

▶

◀

▶

Back

Close

Full Screen / Esc

Printer-friendly Version

Interactive Discussion

controlling variability and absolute levels, *Atmos. Environ.*, 38, 5375–5388, 2004.

Davison, B., Hewitt, C. N., O'Dowd, C. D., Lowe, J. A., Smith, M. H., Schwikowski, M., Baltensperger, U., and Harrison, R. M.: Dimethyl sulphide, methane sulfonic acid and physicochemical aerosol properties in Atlantic air from the United Kingdom to Halley Bay, *J. Geophys. Res.*, 101(D17), 22855–22867, 1996.

Dibb, J. E., Talbot, R. W., Munger, J. W., Jacob, D. J., and Fan, S.-M.: Air-snow exchange of HNO₃ and NO_y at Summit, Greenland, *J. Geophys. Res.*, 103, 3475–3486, 1998.

Dibb, J. E., Arsenault, M., Peterson, M. C., and Honrath, R. E.: Fast nitrogen oxide chemistry in Summit, Greenland snow, *Atmos. Environ.*, 36, 2501–2511, 2002.

Dominé, F. and Shepson, P. B.: Air-snow interactions and atmospheric chemistry, *Science*, 297, 1506–1510, 2002.

Fisher, F. N., King, M. D., and Lee-Taylor, J.: Extinction of UV-visible radiation in wet midlatitude (maritime) snow: Implications for increased NO_x emission, *J. Geophys. Res.*, 110, D21301, doi:10.1029/2005JD005963, 2005.

Grannas, A. M., Jones, A. E., Dibb, J., Ammann, M., Anastasio, C., Beine, H. J., Bergin, M., Bottenheim, J., Boxe, C. S., Carver, G., Chen, G., Crawford, J. H., Dominé, F., Frey, M. M., Guzmán, M. I., Heard, D. E., Helmig, D., Hoffmann, M. R., Honrath, R. E., Huey, L. G., Hutterli, M., Jacobi, H. W., Klán, P., Lefer, B., McConnell, J., Plane, J., Sander, R., Savarino, J., Shepson, P. B., Simpson, W. R., Sodeau, J. R., von Glasow, R., Weller, R., Wolff, E. W., and Zhu, T.: An overview of snow photochemistry: evidence, mechanisms and impacts, *Atmos. Chem. Phys.*, 7, 4329–4373, 2007, <http://www.atmos-chem-phys.net/7/4329/2007/>.

Grenfell, T. C.: A radiative-transfer model for sea ice with vertical structure variations, *J. Geophys. Res.*, 96, 16991–17001, 1991.

Honrath, R. E., Peterson, M. C., Guo, S., Dibb, J. E., Shepson, P. B., and Campbell, B.: Evidence of NO_x Production Within or Upon Ice Particles in the Greenland Snowpack, *Geophys. Res. Lett.*, 26(6), 695–698, 1999.

Honrath, R. E., Lu, Y., Peterson, M. C., Dibb, J. E., Arsenault, M. A., Cullen, N. J., and Steffen, K.: Vertical fluxes of NO_x, HONO, and HNO₃ above the snowpack at Summit, Greenland, *Atmos. Environ.*, 36, 2629–2640, 2002.

Jacobi, H. W., Weller, R., Jones, A. E., Anderson, P. S., and Schrems, O.: Peroxyacetyl nitrate (PAN) concentrations in the Antarctic troposphere measured during the photochemical experiment at Neumayer (PEAN'99), *Atmos. Environ.*, 34, 5235–5247, 2000

Jones, A. E., Weller, R., Wolff, E. W., and Jacobi, H.-W.: Speciation and Rate of Photochemical

**Summertime NO_x
measurements
during the CHABLIS
campaign**

S. J.-B. Bauguitte et al.

[Title Page](#)[Abstract](#)[Introduction](#)[Conclusions](#)[References](#)[Tables](#)[Figures](#)[◀](#)[▶](#)[◀](#)[▶](#)[Back](#)[Close](#)[Full Screen / Esc](#)[Printer-friendly Version](#)[Interactive Discussion](#)

- NO and NO₂ Production in Antarctic Snow, *Geophys. Res. Lett.*, 27(3), 345–348, 2000.
- Jones, A. E., Weller, R., Anderson, P. S., Jacobi, H.-W., Wolff, E. W., Schrems, O., and Miller, H.: Measurements of NO_x emissions from the Antarctic snowpack, *Geophys. Res. Lett.*, 28(8), 1499–1502, 2001.
- 5 Jones, A. E. and Wolff, E. W.: An analysis of the oxidation potential of the South Pole boundary layer and the influence of stratospheric ozone depletion, *J. Geophys. Res.*, 108(D18), 4565, doi:10.1029/2003JD003379, 2003.
- Jones, A. E., Wolff, E. W., Ames, D., Bauguitte, S. J.-B., Clemishaw, K. C., Fleming, Z., Mills, G. P., Saiz-Lopez, A., Salmon, R. A., Sturges, W. T., and Worton, D. R.: The multi-seasonal
10 NO_y budget in coastal Antarctica and its link with surface snow and ice core nitrate: results from the CHABLIS campaign, *Atmos. Chem. Phys. Discuss.*, 7, 4127–4163, 2007, http://www.atmos-chem-phys-discuss.net/7/4127/2007/.
- Jones, A. E., Wolff, E. W., Salmon, R. A., Bauguitte, S. J.-B., Roscoe, H. K., Anderson, P. S., Ames, D., Clemishaw, K. C., Fleming, Z. L., Bloss, W. J., Heard, D. E., Lee, J. D., Read, K. A., Hamer, P., Shallcross, D. E., Jackson, A. V., Walker, S. L., Lewis, A. C., Mills, G. P.,
15 Plane, J. M. C., Saiz-Lopez, A., Sturges, W. T., and Worton, D. R.: Chemistry of the Antarctic Boundary Layer and the Interface with Snow: an overview of the CHABLIS campaign, *Atmos. Chem. Phys.*, 8, 3789–3803, 2008, http://www.atmos-chem-phys.net/8/3789/2008/.
- Lee-Taylor, J. and Madronich, S.: Calculation of actinic fluxes with a coupled atmosphere-snow radiative transfer model, *J. Geophys. Res.*, 107(D24), 4796, doi:10.1029/2002JD002084,
20 2002.
- Leighton, P. A.: Photochemistry of Air Pollution, Vol. IX, in: *Physical Chemistry: A Series of Monographs*, edited by: Hutchinson, E. and Ryssleberghe, P. V., Academic Press, New York, 1961.
- Li, Z., Friedl, R. R., Moore, S. B., and Sander, S. P.: Interaction of peroxydic acid with solid
25 H₂O ice, *J. Geophys. Res.*, 101(D3), 6795–6802, 1996.
- Madronich, S.: Photodissociation in the Atmosphere: 1. Actinic Flux and the Effects of Ground Reflections and Clouds, *J. Geophys. Res.*, 92(D8), 9740–9752, 1987.
- Morin, S., Savarino, J., Frey, M. M., Yan, N., Bekki, S., Bottenheim, J. W., and Martins, J. M. F.: Tracing the Origin and Fate of NO_x in the Arctic Atmosphere Using Stable Isotopes in Nitrate,
30 *Science*, 322, 730–732, doi:10.1126/science.1161910, 2008.
- Oncley, S. P., Buhr, M., Lenschow, D. H., Davis, D., and Semmer, S. R.: Observations of summertime NO fluxes and boundary-layer height at the South Pole during ISCAT 2000 using scalar similarity, *Atmos. Environ.*, 38, 5389–5398, 2004.

Press, W. H., Flannery, B. P., Teukolsky, S. A., and Vetterling, W. T.: Numerical Recipes in C: The Art of Scientific Computing (Second Edition), published by Cambridge University Press, doi:10.2277/0521431085, 1993.

Qiu, R., Green, S. A., Honrath, R. E., Peterson, M. C., Lu, Y., and Dziobak, M.: Measurements of JNO_3^- in snow by nitrate-based actinometry, *Atmos. Environ.*, 36, 2563–2571, 2002.

Read, K. A., Mahajan, A. S., Carpenter, L. J., Evans, M. J., Faria, B. V. E., Heard, D. E., Hopkins, J. R., Lee, J. D., Moller, S. J., Lewis, A. C., Mendes, L., McQuaid, J. B., Oetjen, H., Saiz-Lopez, A., Pilling, M. J., and Plane, J. M. C.: Extensive halogen-mediated ozone destruction over the tropical Atlantic Ocean, *Nature*, 453, 1232–1235, doi:10.1038/nature07035, 2008.

Richter, A., Wittrock, F., Ladstaetter-Weissenmayer, A., and Burrows, J. P.: GOME measurements of stratospheric and tropospheric BrO, *Adv. Space Res.*, 29, 1667–1672, 2002.

Ridley, B., Walega, J., Montzka, D., Grahek, F., Atlas, E., Flocke, F., Stroud, V., Deary, J., Gallant, A., Boudries, H., Bottenheim, J., Anlauf, K., Worthy, D., Sumner, A. L., Splawn, B., and Shepson, P.: Is the Arctic Surface Layer a Source and Sink of NO_x in Winter/Spring?, *J. Atmos. Chem.*, 36, 1–22, 2000.

Ridley, B. A. and Orlando, J. J.: Active Nitrogen in Surface Ozone Depletion Events at Alert during Spring 1998, *J. Atmos. Chem.*, 44, 1–22, 2003.

Ryerson, T. B., Williams, E. J., and Fehsenfeld, F. C.: An efficient photolysis system for fast-response NO_2 measurements, *J. Geophys. Res.*, 105(D21), 26447–26461, 2000.

Sander, S. P., Finlayson-Pitts, B. J., Friedl, R. R., Golden, D. M., Huie, R. E., Keller-Rudek, H., Kolb, C. E., Kurylo, M. J., Molina, M. J., Moortgat, G. K., Orkin, V. L., Ravishankara, A. R., and Wine, P. H.: Chemical Kinetics and Photochemical Data for Use in Atmospheric Studies, Evaluation Number 15, JPL Publication 06-2, Jet Propulsion Laboratory, Pasadena, 2006.

Saiz-Lopez, A., Mahajan, A. S., Salmon, R. A., Bauguitte, S. J.-B., Jones, A. E., Roscoe, H. K., and Plane, J. M. C.: Boundary layer halogens in coastal Antarctica, *Science*, 317, 348–351, doi:10.1126/science.1141408, 2007a.

Saiz-Lopez, A., Chance, K., Liu, X., Kurosu, T. P., and Sander, S. P.: First observations of iodine oxide from space, *Geophys. Res. Lett.*, 34, L12812, doi:10.1029/2007GL030111, 2007b.

Saiz-Lopez, A., Plane, J. M. C., Mahajan, A. S., Anderson, P. S., Bauguitte, S. J.-B., Jones, A. E., Roscoe, H. K., Salmon, R. A., Bloss, W. J., Lee, J. D., and Heard, D. E.: On the vertical distribution of boundary layer halogens over coastal Antarctica: implications for O_3 , HO_x , NO_x and the Hg lifetime, *Atmos. Chem. Phys.*, 8, 887–900, 2008, <http://www.atmos-chem-phys.net/8/887/2008/>.

Summertime NO_x measurements during the CHABLIS campaign

S. J.-B. Bauguitte et al.

Title Page

Abstract

Introduction

Conclusions

References

Tables

Figures

◀

▶

◀

▶

Back

Close

Full Screen / Esc

Printer-friendly Version

Interactive Discussion

- Schönhardt, A., Richter, A., Wittrock, F., Kirk, H., Oetjen, H., Roscoe, H. K., and Burrows, J. P.: Observations of iodine monoxide columns from satellite, *Atmos. Chem. Phys.*, 8, 637–653, 2008, <http://www.atmos-chem-phys.net/8/637/2008/>.
- Seinfeld, J. H. and Pandis, S. N.: *Atmospheric Chemistry and Physics: From Air Pollution to Climate Change*, John Wiley & Sons, Inc., 1998.
- Simpson, W. R., von Glasow, R., Riedel, K., Anderson, P., Ariya, P., Bottenheim, J., Burrows, J., Carpenter, L. J., Frieß, U., Goodsite, M. E., Heard, D., Hutterli, M., Jacobi, H.-W., Kaleschke, L., Neff, B., Plane, J., Platt, U., Richter, A., Roscoe, H., Sander, R., Shepson, P., Sodeau, J., Steffen, A., Wagner, T., and Wolff, E.: Halogens and their role in polar boundary-layer ozone depletion, *Atmos. Chem. Phys.*, 7, 4375–4418, 2007, <http://www.atmos-chem-phys.net/7/4375/2007/>.
- Sjostedt, S. J., Huey, L. G., Tanner, D. J., Peischl, J., Chen, G., Dibb, J. E., Lefer, B., Hutterli, M. A., Beyersdorf, A. J., Blake, N. J., Blake, D. R., Sueper, D., Ryerson, T., Burkhardt, J., and Stohl, A.: Observations of hydroxyl and the sum of peroxy radicals at Summit, Greenland during summer 2003, *Atmos. Environ.*, 41, 5122–5137, 2007.
- von Glasow, R., von Kuhlmann, R., Lawrence, M. G., Platt, U., and Crutzen, P. J.: Impact of reactive bromine chemistry in the troposphere, *Atmos. Chem. Phys.*, 4, 2481–2497, 2004, <http://www.atmos-chem-phys.net/4/2481/2004/>.
- Weller, R., Jones, A. E., Wille, A., Jacobi, H.-W., McIntyre, H. P., Sturges, W. T., Huke, M., and Wagenbach, D.: Seasonality of reactive nitrogen oxides (NO_x) at Neumayer Station, Antarctica, *J. Geophys. Res.*, 107(D23), 4673, doi:10.1029/2002JD002495, 2002.
- Wolff, E. W.: Nitrate in polar ice, in: *Ice Core Studies of Global Biogeochemical Cycles*, NATO ASI Ser., vol. 130, edited by: Delmas, R. J., Springer-Verlag, New York, 195–224, 1995.
- Wolff, E. W., Jones, A. E., Martin, T. J., and Grenfell, T. C.: Modelling photochemical NO_x production and nitrate loss in the upper snow pack of Antarctica, *Geophys. Res. Lett.*, 29(20), 1944, doi:10.1029/2002GL015823, 2002.
- Wolff, E. W., Jones, A. E., Bauguitte, S. J.-B., and Salmon, R. A.: The interpretation of spikes and trends in concentration of nitrate in polar ice cores, based on evidence from snow and atmospheric measurements, *Atmos. Chem. Phys.*, 8, 5627–5634, 2008, <http://www.atmos-chem-phys.net/8/5627/2008/>.
- Yang, X., Cox, R. A., Warwick, N. J., Pyle, J. A., Carver, G. D., O'Connor, F. M., and Savage, N.: Tropospheric bromine chemistry and its impact on ozone: A model study, *J. Geophys. Res.*, 110, D23311, doi:10.1029/2005JD006244, 2005.

**Summertime NO_x
measurements
during the CHABLIS
campaign**S. J.-B. Bauguitte et al.

Title Page

Abstract

Introduction

Conclusions

References

Tables

Figures

◀

▶

◀

▶

Back

Close

Full Screen / Esc

Printer-friendly Version

Interactive Discussion

Summertime NO_x measurements during the CHABLIS campaign

S. J.-B. Bauguitte et al.

Table 1. Summary of CL detector performance parameters, and nominal precision and accuracy of one minute NO_x mixing ratios below 20 pptv. The NO₂ systematic error includes the contribution due to the systematic error in NO.

	NO	NO ₂
NO sensitivity, Hz/pptv	4.2	2.5
Background count rate, Hz	300–400	300–400
Reaction chamber vacuum, Torr	10	10
Detector flow-rate, std L min ⁻¹	1	1
Artefact, pptv	–2	–6
NO ₂ photolytic CE, %	N/a	55–60
Random 1σ standard error, pptv	±1.0	±3.0
Systematic error, pptv	±1.3	±3.3
Limit of detection, pptv	1	4

[Title Page](#)
[Abstract](#)
[Introduction](#)
[Conclusions](#)
[References](#)
[Tables](#)
[Figures](#)
[Back](#)
[Close](#)
[Full Screen / Esc](#)
[Printer-friendly Version](#)
[Interactive Discussion](#)

Table 2. Summary of NO_x flux measurements in Arctic and Antarctic studies.

Location	Date	NO _x flux, molec cm ⁻² s ⁻¹	Reference
<i>Antarctic measurements</i>			
Neumayer 70°39' S, 8°15' W, 42 m	5–7 Feb 1999	~3 (+0.3/–0.9)×10 ⁸ (noon maxima)	Jones et al. (2001)
South Pole 2835 m	26–30 Nov 2000	3.9±0.4×10 ⁸ (average over period)	Oncley et al. (2004)
Halley V 75°35' S, 26°40' W, 37 m	1 Feb 2005 2 Feb 2005 4 Feb 2005	1.7×10 ⁸ daily mean 3.4×10 ⁸ daily mean 2.2×10 ⁸ daily mean	this study
<i>Arctic measurements</i>			
Summit, Greenland 72°36' N, 38°30' W, 3200 m	5 June–3 July 2001	2.5×10 ⁸ (daily average)	Honrath et al. (2002)
Alert, Nunavut, Canada, 82° 30' N, 62° 18' W, 220 m	9–25 April 2000	≥6.7×10 ⁸ (noon maxima)	Beine et al. (2002)

Summertime NO_x measurements during the CHABLIS campaign

S. J.-B. Bauguitte et al.

Title Page

Abstract

Introduction

Conclusions

References

Tables

Figures

⏪

⏩

◀

▶

Back

Close

Full Screen / Esc

Printer-friendly Version

Interactive Discussion

Summertime NO_x measurements during the CHABLIS campaign

S. J.-B. Bauguitte et al.

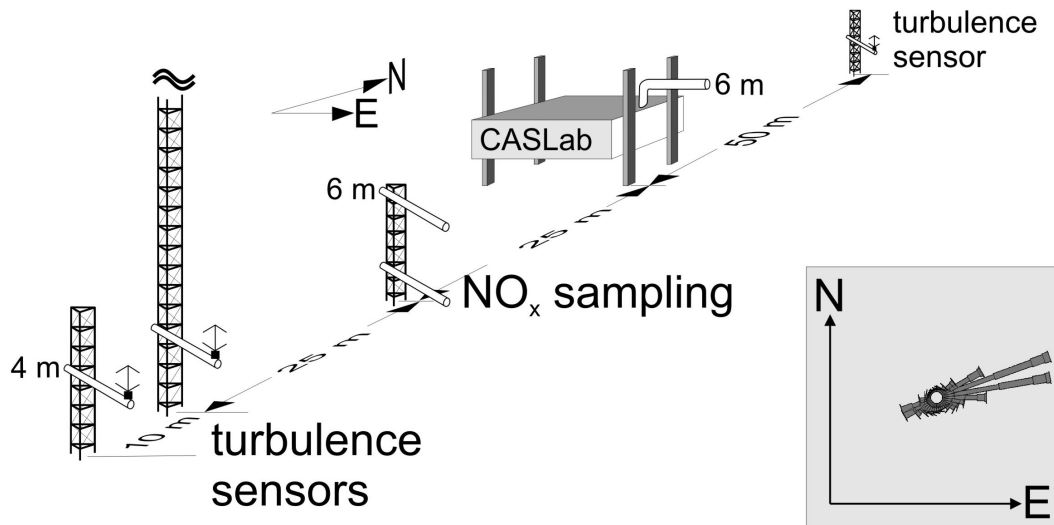


Fig. 1. Schematic of location of inlets and turbulence sensors used for NO_x flux measurements during CHABLIS. The lower NO_x sampling inlet, situated 25 m South of the CASLab, is 1.5 m high. The inset shows the mean wind rose at Halley.

[Title Page](#)[Abstract](#)[Introduction](#)[Conclusions](#)[References](#)[Tables](#)[Figures](#)[◀](#)[▶](#)[◀](#)[▶](#)[Back](#)[Close](#)[Full Screen / Esc](#)[Printer-friendly Version](#)[Interactive Discussion](#)

**Summertime NO_x
measurements
during the CHABLIS
campaign**

S. J.-B. Bauguitte et al.

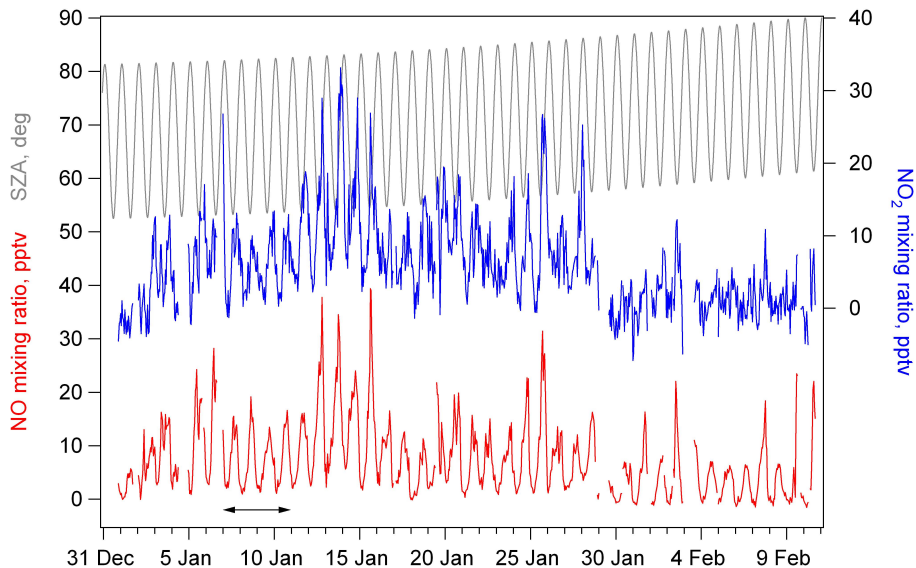


Fig. 2. Mixing ratios (pptv) of NO (red, left-hand scale), NO₂ (blue, right-hand scale) and solar zenith angle (grey, left-hand scale) from 1 January to 10 February 2005. These NO and NO₂ values are one hourly means of the one minute pollution-filtered data. The black arrow indicates the four-day blizzard conditions, when wind speeds in excess of 15 m s^{-1} and blowing snow were experienced.

[Title Page](#)[Abstract](#)[Introduction](#)[Conclusions](#)[References](#)[Tables](#)[Figures](#)[◀](#)[▶](#)[◀](#)[▶](#)[Back](#)[Close](#)[Full Screen / Esc](#)[Printer-friendly Version](#)[Interactive Discussion](#)

**Summertime NO_x
measurements
during the CHABLIS
campaign**

S. J.-B. Bauguitte et al.

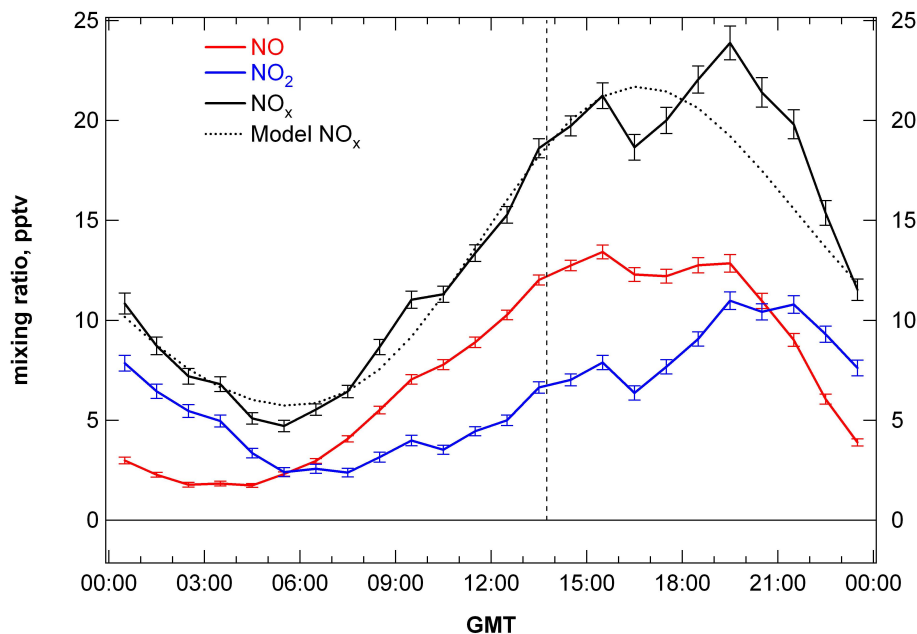


Fig. 3. Hourly mean diurnal cycle of NO (red), NO₂ (blue) and NO_x (black) for 1 January to 10 February 2005, compiled from the one minute pollution-filtered master dataset. Error bars are 2 σ standard (random) errors of each hourly mean. The dotted black line (Model NO_x) corresponds to the Steady State NO_x calculations (see text). The vertical dashed line indicates local noon, 13:45 h.

[Title Page](#)[Abstract](#)[Introduction](#)[Conclusions](#)[References](#)[Tables](#)[Figures](#)[⏪](#)[⏩](#)[◀](#)[▶](#)[Back](#)[Close](#)[Full Screen / Esc](#)[Printer-friendly Version](#)[Interactive Discussion](#)

**Summertime NO_x
measurements
during the CHABLIS
campaign**

S. J.-B. Bauguitte et al.

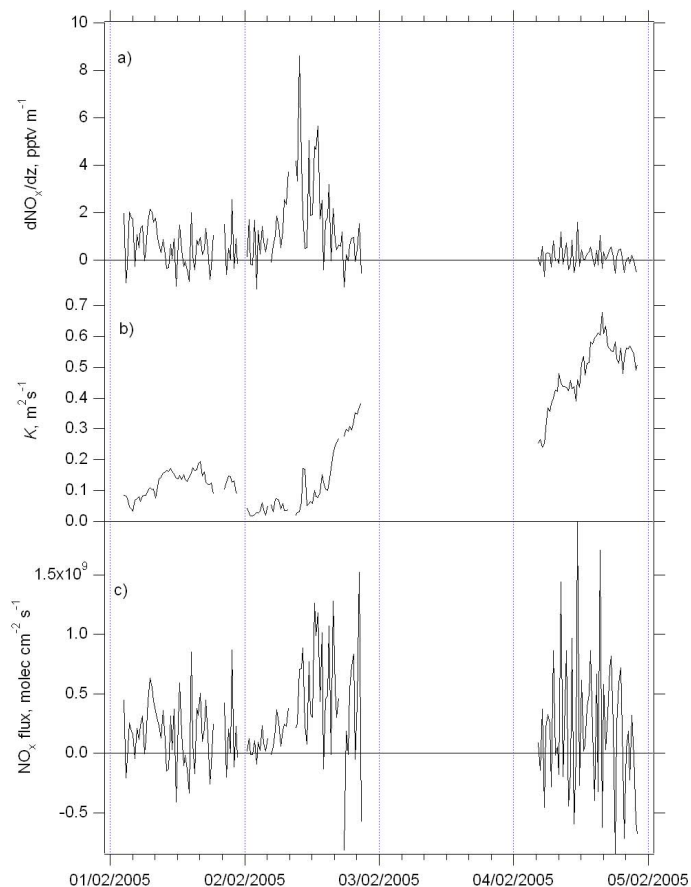
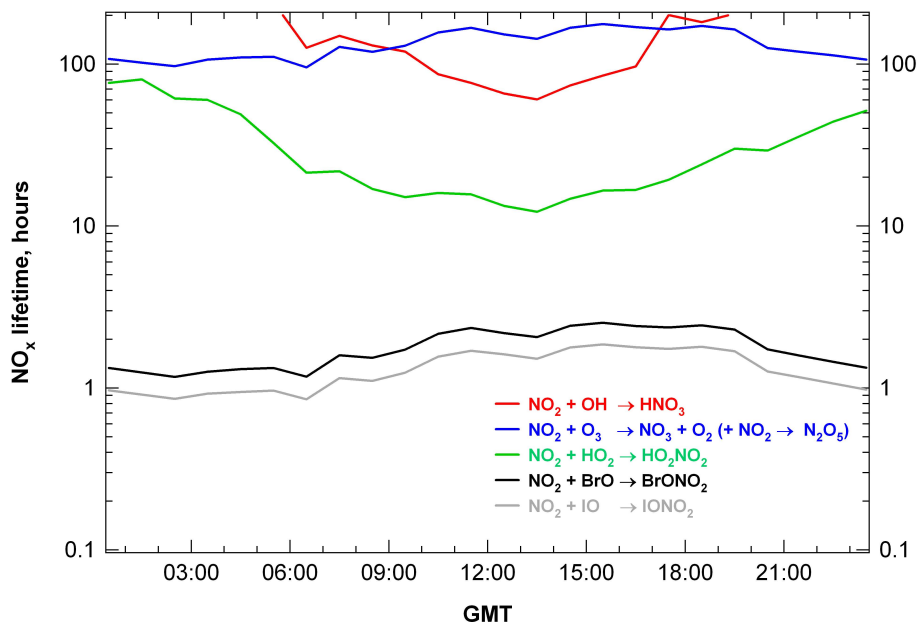


Fig. 4. (a) 20 min average NO_x gradients ($\frac{\partial \text{NO}_x}{\partial z}$) estimated from the 1.5 and 6 m high inlets NO_x measurements; (b) 20 min average surface diffusivities (K) estimated from the friction velocities U_* at 4 m height; (c) 20 min average NO_x fluxes expressed as the product $\frac{\partial \text{NO}_x}{\partial z} \times K$.

[Title Page](#)[Abstract](#)[Introduction](#)[Conclusions](#)[References](#)[Tables](#)[Figures](#)[◀](#)[▶](#)[◀](#)[▶](#)[Back](#)[Close](#)[Full Screen / Esc](#)[Printer-friendly Version](#)[Interactive Discussion](#)

**Summertime NO_x
measurements
during the CHABLIS
campaign**

S. J.-B. Bauguitte et al.

**Fig. 5.** Diurnal NO_x lifetimes, derived from calculations of known NO₂ oxidation-loss pathways.[Title Page](#)[Abstract](#)[Introduction](#)[Conclusions](#)[References](#)[Tables](#)[Figures](#)[◀](#)[▶](#)[◀](#)[▶](#)[Back](#)[Close](#)[Full Screen / Esc](#)[Printer-friendly Version](#)[Interactive Discussion](#)

**Summertime NO_x
measurements
during the CHABLIS
campaign**

S. J.-B. Bauguitte et al.

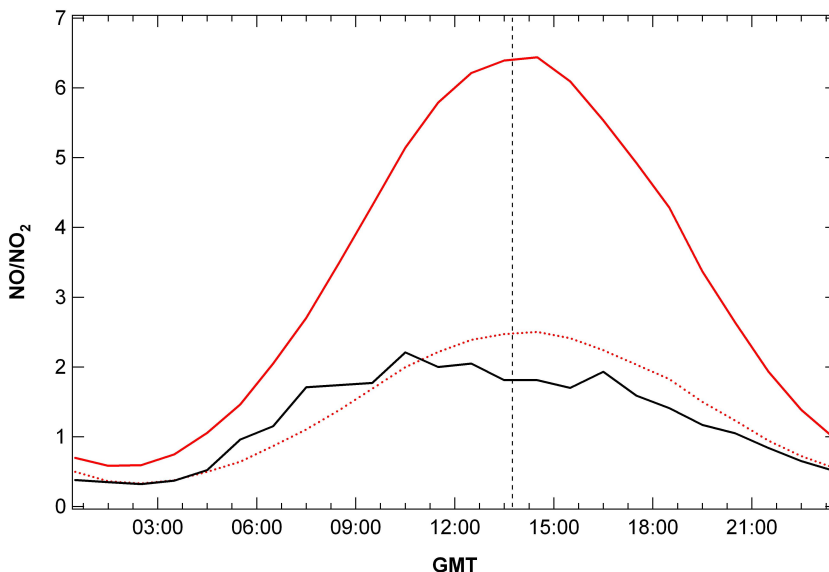


Fig. 6. Solid black line: hourly mean diurnal cycle of observed NO/NO₂ ratios. Solid red line: NO/NO₂ ratios calculated using “classic” Leighton relationship (ozone as sole oxidant). Dotted red line: NO/NO₂ ratios calculated using “extended” Leighton relationship (ozone plus diurnally varying IO and BrO oxidants). The vertical dashed line indicates local noon, 13:45 h.

[Title Page](#)[Abstract](#)[Introduction](#)[Conclusions](#)[References](#)[Tables](#)[Figures](#)[⏪](#)[⏩](#)[◀](#)[▶](#)[Back](#)[Close](#)[Full Screen / Esc](#)[Printer-friendly Version](#)[Interactive Discussion](#)